



Simple heteroaryl modifications in the 4,5-diarylisoxazol-3-carboxylic acid scaffold favorably modulates the activity as dual mPGES-1/5-LO inhibitors with *in vivo* efficacy

Tuğba Gürses^a, Abdurrahman Olğaç^a, Ulrike Garscha^b, Tuğçe Gür Maz^a, Nur Banu Bal^c, Orhan Uludağ^c, Burcu Çalışkan^a, Ulrich S. Schubert^{d,e}, Oliver Werz^{b,d}, Erden Banoglu^{a,*}

^a Department of Pharmaceutical Chemistry, Faculty of Pharmacy, Gazi University, Yenimahalle, 06560 Ankara, Turkey

^b Department of Pharmaceutical/Medicinal Chemistry, Institute of Pharmacy, Friedrich-Schiller-University Jena, Philosophenweg 14, D-7743 Jena, Germany

^c Department of Pharmacology, Faculty of Pharmacy, Gazi University, Yenimahalle, 06560 Ankara, Turkey

^d Jena Center for Soft Matter (JCSM), Friedrich Schiller University Jena, Philosophenweg 7, 07743 Jena, Germany

^e Laboratory of Organic and Macromolecular Chemistry (IOMC), Friedrich Schiller University Jena, Humboldtstrasse 10, D-07743 Jena, Germany

ARTICLE INFO

Keywords:

Microsomal prostaglandin E₂ synthase-1
5-lipoxygenase
5-lipoxygenase-activating protein
Isoxazole
Inflammation

ABSTRACT

Microsomal prostaglandin E₂ synthase-1 (mPGES-1), 5-lipoxygenase (5-LO) and 5-lipoxygenase-activating protein (FLAP) are key for biosynthesis of proinflammatory lipid mediators and pharmacologically relevant drug targets. In the present study, we made an attempt to explore the role of small heteroaromatic fragments on the 4,5-diarylisoxazol-3-carboxylic acid scaffold, which are selected to interact with focused regions in the active sites of mPGES-1, 5-LO and FLAP. We report that the simple structural variations on the benzyloxyaryl side-arm of the scaffold significantly influence the selectivity against mPGES-1, 5-LO and FLAP, enabling to produce multi-target inhibitors of these protein targets, exemplified by compound 18 (IC₅₀ mPGES-1 = 0.16 μM; IC₅₀ 5-LO = 0.39 μM) with *in vivo* efficacy in animal model of inflammation. The computationally modeled binding structures of these new inhibitors for three targets provide clues for rational design of modified structures as multi-target inhibitors. In conclusion, the simple synthetic procedure, and the possibility of enhancing the potency of this class of inhibitors through structural modifications pave the way for further development of new multi-target inhibitors against mPGES-1, 5-LO and FLAP, with potential application as anti-inflammatory agents.

1. Introduction

Drug discovery efforts on effective relief of chronic inflammatory conditions including pain have been an ongoing challenge for medicinal chemists for many years. Traditionally, cyclooxygenase (COX)-inhibiting non-steroidal anti-inflammatory drugs (NSAIDs) represent an important therapeutic class for the alleviation of pain and inflammation associated with a number of pathologies such as arthritis, Alzheimer's disease, atherosclerosis, and cancer. However, the prolonged utilization of these drugs may limit their therapeutic benefits due to severe gastrointestinal or cardiovascular side effects [1,2]. Therefore, there is still growing interest for alternative pharmacological approaches for the discovery of improved anti-inflammatory drugs devoid of the side effects inherent to traditional NSAIDs.

The microsomal prostaglandin E₂ synthase-1 (mPGES-1) has been in

the center of extensive research efforts for next-generation NSAIDs with the aim of circumventing COX-related side effects [3,4]. mPGES-1 is the terminal enzyme in the arachidonic acid (AA) cascade, which is functionally coupled to COX-2, and catalyzes the transformation of prostaglandin (PG)H₂ to pro-inflammatory PGE₂ (Fig. 1) [5]. Since mPGES-1 as well as COX-2 is strongly up-regulated under inflammatory conditions, its inhibition would selectively interfere with the production of mPGES-1-derived pro-inflammatory PGE₂ while keeping the biosynthesis of house-keeping PGs unaffected (Fig. 1). To date, although a broad spectrum of *in vitro* SAR data on numerous classes of mPGES-1 inhibitors has been reported, only a limited number of mPGES-1 inhibitors are available with *in vivo* analgesic and anti-inflammatory efficacy in animal models [5,6]. In addition, two mPGES-1 inhibitors, LY3023703 (1) by Eli Lilly and GRC-27864 (2) from Glenmark Pharmaceuticals, completed Ph-I clinical studies for the treatment of

* Corresponding author.

E-mail address: banoglu@gazi.edu.tr (E. Banoglu).

<https://doi.org/10.1016/j.bioorg.2021.104861>

Received 4 October 2020; Received in revised form 2 January 2021; Accepted 21 March 2021

Available online 24 March 2021

0045-2068/© 2021 Elsevier Inc. All rights reserved.

inflammation and pain [7–9]. Therefore, selective inhibition of mPGES-1 preserves its status to be a promising approach for the design of effective anti-inflammatory drugs lacking NSAID related side effects.

Besides COXs and mPGES-1, 5-lipoxygenase (5-LO) and 5-LO-activating protein (FLAP) are intensively studied therapeutic targets, which are key for production of leukotrienes (LTs) from AA, and involved in inflammatory and allergic processes (Fig. 1) [10,11]. 5-LO in conjunction with FLAP catalyzes the initial step of LT biosynthesis by converting AA to instable LTA_4 , which in turn is used to produce chemotactic LTB_4 and vasoactive cysteinyl-LTs by the action of LTA_4 hydrolase and LTC_4 synthase, respectively. Preclinical and a few clinical studies on the inhibition of LT pathway have demonstrated several beneficial pharmacological effects, such as suppression of inflammation and allergy-induced bronchoconstriction [11]. Although a vast number of 5-LO inhibitors have been developed for anti-inflammatory purposes, they have not reached the pharmaceutical market for reasons such as lack of selectivity and mechanism-based side effects. So far, zileuton (3) is still the only compound, which is approved as drug for treatment of asthma. In this respect, FLAP inhibitors as broad-spectrum anti-LT agents are more advanced, and several of them, i.e., fibroflapon (4, GSK2190915), AZD5718 (5) and BI665915 (6) were reported to be in various stages of preclinical and clinical studies for inflammation-related diseases such as asthma, chronic obstructive pulmonary disease (COPD) and atherosclerosis (Fig. 2) [12–14].

Meanwhile, single therapy with COX-inhibiting NSAIDs was shown to elevate levels of chemotactic LTB_4 , which also contributes to the inflammatory process and also to the gastric toxicity observed with NSAIDs use [15]. Several lines of studies indicated that dual inhibitors, which are able to block equally well both the COX and 5-LO pathways might have superior anti-inflammatory activity and more gastrointestinal safety as compared to the therapy with single inhibitors of each pathway [15]. Indeed, licofelone (7), a balanced inhibitor of mPGES-1, FLAP and COX-1, have demonstrated higher anti-inflammatory activity with greater safety profile and has been evaluated in phase-III clinical studies [16], indicating that multitarget strategy in the AA pathway might be the most promising therapeutic solution for inflammatory diseases.

Within the frame of our research efforts towards the development of better anti-inflammatory drug candidates targeting 5-LO, FLAP and mPGES-1 [17–23], we previously identified novel dual inhibitors of PG and LT pathway based on the core structure of 4,5-diarylisoaxazole-3-carboxylic acid (8) targeting FLAP and 5-LO [24,25]. Our initial studies disclosed that the installation of various substituted phenyl or quinoline rings as R groups on 8 tangled the selectivity of this core structure between 5-LO (8a) and FLAP (8b) (Fig. 2) [24]. Follow up studies with 8b

also demonstrated that this quinolinyl derivative (8b) was able to intervene with PGE_2 production by targeting mPGES-1, therefore resulting in a multitarget compound within pro-inflammatory lipid mediator biosynthesis. Encouraged by the promising in vitro pharmacological profile of this multitarget inhibitor 8b (BRP-187) [25], we herein randomly explored the effectiveness of various commercially available heteroaromatic residues in place of quinoline ring in BRP-187 to better understand the role of this part with regard to the activity tangling among the target proteins mPGES-1, 5-LO and FLAP (see Table 1).

2. Results and discussion

2.1. Chemistry

Synthesis of compounds 17–26 was performed by a multi-step reaction (Scheme 1) according to the previously published procedures [24]. In brief, commercially available p-hydroxyacetophenone was protected by benzylation (1) prior to the reaction with diethyl oxalate to generate keto-enol ester 2. The obtained keto-enol ester 2 was refluxed with hydroxylamine in ethanol to produce isoxazole intermediate 3, which was brominated at 4-position (4) with *N*-bromosuccinimide in the presence of a catalytic amount of ceric ammonium nitrate. The resulting brominated derivative underwent a palladium-catalyzed Suzuki cross-coupling reaction with p-chlorophenylboronic acid to afford 5. Debenzylation of 5 by catalytic hydrogenation furnished the starting intermediate 6, which was subsequently used to produce desired final compounds 17–26 through first the alkylation of the phenolic hydroxyl and then the hydrolysis of the ester group.

2.2. Analysis of bioactivity and SAR

To assess the inhibitory potential of the title compounds on mPGES-1 activity (transformation of PGH_2 to PGE_2), a cell-free assay using the microsomal fractions of interleukin (IL)-1 β -stimulated A549 cells as the enzyme source was applied [26]. However, previous studies on various mPGES-1 inhibitors demonstrated that they may potentially interact with 5-LO or FLAP, therefore producing compounds with multitarget properties within the AA cascade [26–30]. In addition, it is suggested that simultaneous interference with the formation of both LTs and PGE_2 might offer added value over single interference with any of these targets in terms of higher anti-inflammatory efficacy and with reduced side effects, i.e., the almost complete lack of gastric toxicity, the most troublesome side effect of NSAIDs [15,31]. Biosynthesis of LTs is initiated by cytosolic phospholipase A₂ (cPLA₂)-mediated release of AA, which is

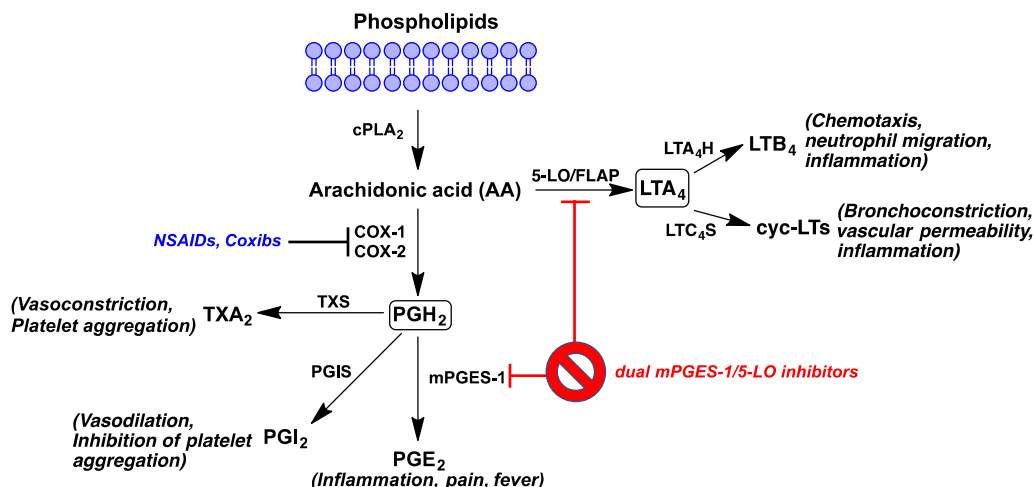


Fig. 1. Schematic illustration of the arachidonic acid cascade. Targeted enzymes (mPGES-1 and 5-LO/FLAP) are indicated.

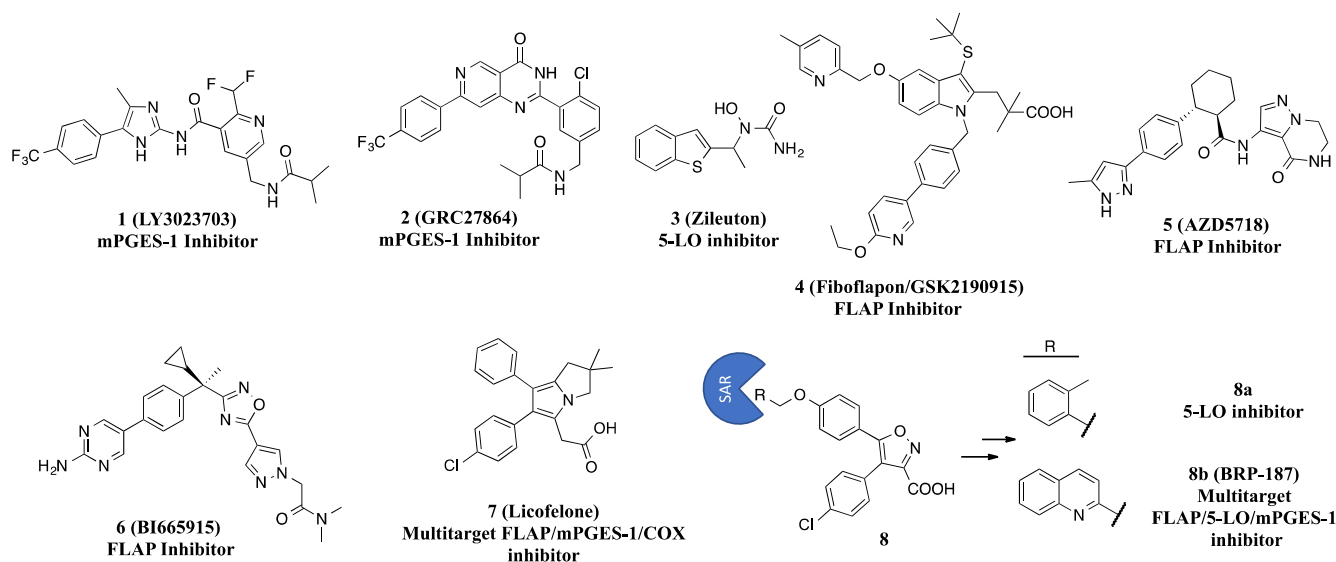


Fig. 2. Representative chemical structures of FLAP, mPGES-1 and multi-target inhibitors.

Table 1
Inhibition of mPGES-1 and 5-LO by 4,5-diarylisoxazole-3-carboxylic acid derivatives.

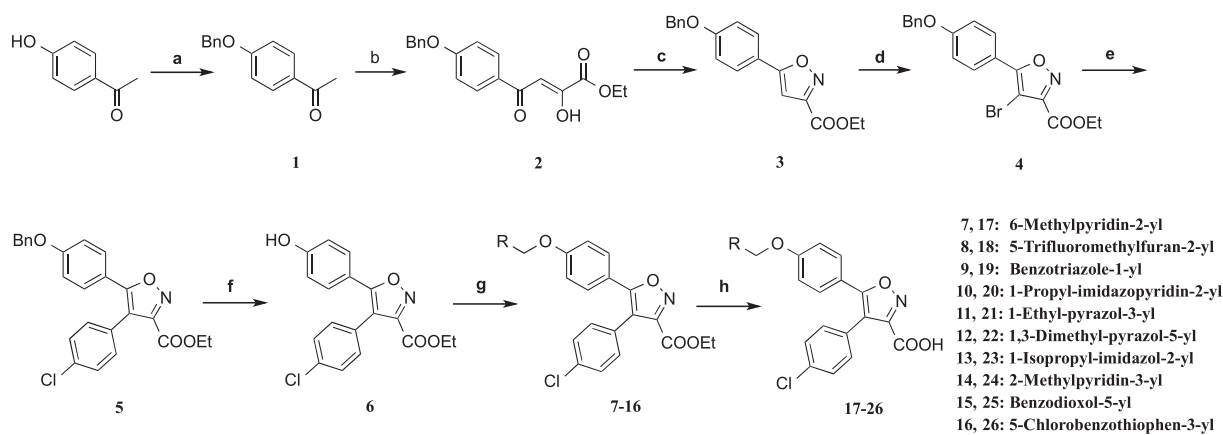
R	mPGES-1 r.a. @ 10 μ M (%)	mPGES-1 IC ₅₀ [μ M]	IC ₅₀ [μ M]	
			PMNL	Purified 5- LO
	44.7 \pm 4.0	0.25 \pm 0.04	0.3 \pm 0.07	2.8 \pm 0.8
	34.4 \pm 0.8	0.16 \pm 0.02	2.7 \pm 0.5	0.39 \pm 0.1
	39.6 \pm 4.9	0.16 \pm 0.07	>10	>10
	68.4 \pm 8.6	>10	>10	3.1 \pm 0.1
	90.8 \pm 2.8	>10	0.8 \pm 0.1	>10
	85.0 \pm 6.2	>10	2.2 \pm 0.8	>10
	102.5 \pm 9.0	>10	>10	>10
	101.8 \pm 8.3	>10	2.7 \pm 0.3	5.1 \pm 3.3
	43.7 \pm 6.0	3.1 \pm 0.3	1.7 \pm 0.3	2.5 \pm 1.2
	24.8 \pm 1.6	0.21 \pm 0.07	1.1 \pm 0.6	1.5 \pm 0.8
MK886	–	2.2	0.08	–
Zileuton	–	–	–	0.6

subsequently converted to LTA₄ by activated 5-LO with the aid of FLAP that may facilitate access of 5-LO to AA (Fig. 1) [32]. It is known that FLAP is essential for cellular 5-LO product formation from endogenous AA, but it is dispensable for 5-LO activity in cell-free systems [33,34]. Therefore, we also analyzed the inhibition of 5-LO product formation in a “FLAP-independent” cell-free assay using purified human recombinant 5-LO enzyme as well as in a “FLAP-dependent” cell-based assay using

human neutrophils. Analyzed 5-LO products include 5-H(P)ETE and all *trans*-isomers of LTB₄, as well as LTB₄ in intact cells. MK-886 with an IC₅₀ = 2 μ M for mPGES-1 [35] and zileuton with an IC₅₀ = 0.58 μ M (cell-based) and 0.80 (cell-free) for 5-LO [24] used as reference drugs.

In a first screening round, all compounds were tested against mPGES-1 at a concentration of 10 μ M. As shown in Table 1, compounds 17–19 and 26 profoundly inhibited mPGES-1 activity, however all other derivatives (20–25) were not significantly active at a concentration of 10 μ M. More detailed analysis of 17–19 and 26 in concentration–response studies revealed IC₅₀ values in the range of 0.16–0.25 μ M (Table 1), which clearly outperforms MK886, indicating that the heteroaryl fragments might have a strong influence for directing the mPGES-1 inhibitory activity in this scaffold. Intriguingly, among these heteroaryl-substituted compounds (17–26), the 5-CF₃-furan-substituted 18, the most active mPGES-1 inhibitor (IC₅₀ = 0.16 μ M), was also the most potent 5-LO inhibitor with IC₅₀ = 0.39 μ M, demonstrating the most favorable dual inhibitor pharmacological profile with sub-micromolar activity. In regard to 5-LO inhibition, installation of 6-CH₃-pyridine (17), benzotriazole (19), benzodioxol (25) and 5-Cl-benzothiophene (26) as heteroaromatic counterparts led to decreased activities against 5-LO enzyme (IC₅₀ = 1.5 - >10 μ M), while keeping the potency against mPGES-1 (IC₅₀ = 0.16–0.25 μ M). Among them, the benzotriazole 19 behaved as a selective mPGES-1 inhibitor with an IC₅₀ of 0.16 μ M (Table 1). Surprisingly, replacement of benzotriazole in 19 with 1-propyl-imidazopyridine resulted in a derivative (20) with selective inhibitory activity against isolated 5-LO. Another interesting observation made with the replacement of 6-CH₃-pyridin-2-yl in 17 (dual mPGES-1/5-LO inhibitor) with 2-CH₃-pyridin-3-yl resulting in an analogue 24 with selectivity against 5-LO pathway. A significant and concentration-dependent suppression of cellular 5-LO product biosynthesis was found for 1-ethyl-pyrazole 21 (IC₅₀ = 0.4 μ M) and also for 1,3-dimethyl-pyrazole 22 (IC₅₀ = 2.2 μ M), although these compounds hardly inhibited 5-LO and mPGES-1 in the cell-free assay. This suggests that for suppression of 5-LO product formation in intact cells, 21 and 22 may primarily act at other targets than the 5-LO enzyme, presumably on FLAP.

All in all, based on the observed biological activity data, 18 is the most efficient dual inhibitor of mPGES-1 and 5-LO activities, 21 and 22 may act as direct FLAP inhibitors, while 19 and 20 behave as potent and selective mPGES-1 and 5-LO inhibitors, respectively. Besides 18, compounds 17, 25 and 26 also act as dual inhibitors of mPGES-1 and 5-LO activity, although with a moderate inhibitory activity on 5-LO. Hence, we aimed to rationalize the biological results through molecular



Scheme 1. Reagents and conditions: (a) Benzylchloride, K_2CO_3 , MeCN, reflux; (b) $(CO_2Et)_2$, Na, EtOH, rt; (c) $NH_2OH.HCl$, EtOH, reflux; (d) NBS, CAN, AcCN; (e) 4-Chlorophenylboronic acid, $Pd(PPh_3)_2Cl_2$, Na_2CO_3 , 1,4-Dioxane, H_2O ; (f) Pd/C , H_2 , HCl, EtOH:THF (3:2); (g) appropriate halides, K_2CO_3 , MeCN, reflux; (h) $LiOH.H_2O$, THF: H_2O (1:1).

modelling studies.

2.3. Molecular modeling studies

2.3.1. Docking studies

Molecular docking studies were conducted on the reported crystal structures of mPGES-1 (PDB code 5TL9 [36]), 5-LO (PDB code 3O8Y [37]) and FLAP (PDB code 2Q7M [38]) for all the molecules in this study to reveal the potential molecular interactions between ligands and proteins. The interaction regions within the active site can be divided into four sub-pockets for these series of molecules, i.e., one hydrophilic and three hydrophobic sub-pockets, and docking-based common interaction analysis against mPGES-1, 5-LO, and FLAP is summarized in Table 2. It should be noted that the isoxazole-5-phenyl group is facing to the lipophilic tail of membrane for mPGES-1, which is not included in the docking studies. The predicted binding modes of the compounds with mPGES-1 (Fig. 3), 5-LO (Fig. 4) and FLAP (Fig. 5 and S1) reveal that the head carboxylate groups form electrostatic interactions (i.e., salt bridges) with basic amino acids, and the chlorophenyl moieties are directed to a hydrophobic groove making hydrophobic contacts, π - π stacking and van der Waals (vdW) interactions. However, small structural variations at the heteroaryl part apparently have complex consequences for compounds with distinct selectivity. Positioning the heteroaromatic moieties in a correct orientation is beneficial to establish the required hydrophobic contacts as well as filling the binding pocket of three proteins. Accordingly, the predicted binding modes of the active compounds were similar with regard to the observed sub-pocket

Table 2

Molecular docking-based common multi-target interaction analysis of 4,5-diarylisoxazole-3-carboxylic acid derivatives.

Fragment	Target			Interaction Type
	mPGES-1	5-LO	FLAP	
Carboxylate	ARG52	HIS600	HIS28	Ionic Interaction
Hydrophilic P.	HIS53		LYS116	
p-chlorophenyl	LEU39	LEU414	LYS116	vdW Interaction
Hydrophobic-1P.		ALA603	LEU120	
	HIS53	TYR181		π - π Stacking
Isoxazole-5-phenyl	Membrane	GLN363	ILE113	vdW Interaction
Hydrophobic-2P.		PHE421		
		ASN425		
		LEU607		
Heteroaryl	ILE32	LEU368	VAL61	vdW Interaction
Hydrophobic-3P.	TYR130	ALA410	ALA63	
	GLN134	HIS372	TYR112	

* not present in docking study.

interactions but divergent and inconclusive for less potent derivatives.

The binding specificity of the active compounds for each of their corresponding protein was conferred by taking into consideration of the binding interactions as described in the following for each target. For instance, while carboxylate, p-chlorophenyl and isoxazole-5-phenyl moieties of 17–19, 25 and 26 shared similar binding interactions at the mPGES-1 active site, different heteroaryl fragments generated slight changes in their binding modes. While isoxazole-5-phenyl core of the compounds are found facing through the membrane location, carboxylate fragments make ionic interactions with ARG52 and HIS53 amino acids, p-chlorophenyl moieties form Van der Waals interactions with LEU39 and π - π stacking with HIS53 (Fig. 3). In addition, compounds 17–19 and 26 generated only hydrophobic contacts in their related sub-pocket, while compound 25 formed a new hydrogen bond with GLN134 that slightly weakened the hydrophobic interaction network in that region resulting in an undesired decrease to the compound's inhibitory effect for mPGES-1.

For 5-LO, compounds 17, 18, 24–26 make ionic interactions to HIS600 with their carboxylate moiety and share the same interaction network with p-chlorophenyl group with residues TYR181, LEU414 and ALA603. Meanwhile, the isoxazole-5-phenyl core makes Van der Waals interactions with alkyl chains of the surrounding amino acids and hydrogen bond with ASN425, heteroaryl fragments show minor differences in their binding orientations. Although these fragments mainly form hydrophobic contacts with the surrounding residues, 5- CF_3 -furan part in 18 showed an orthogonal multipolar interaction with GLN363 (Fig. 4).

Most of the interaction network with carboxylate and p-chlorophenyl moieties were also shared between the compounds 21–22 and FLAP (Fig. 5 and S1). For example, while carboxylate groups form ionic interaction with LYS116 and isoxazole-5-phenyl core forms hydrophobic interactions with ILE113, p-chlorophenyl moiety makes Van der Waals interactions with LYS116 and LEU120 amino acids. Heteroaryl fragments form hydrophobic interactions with surrounding amino acids (Fig. 5). The docking runs for compounds 20 and 23, which contain o-substituents on the heteroaryl moiety, were failed and did not generate any docking result for all targets, due to their increased volume that sterically blocked fitting the compounds while keeping the proteins' active site rigid. Additionally, an interaction matrix together with the IC_{50} values is given for the reported compounds and targets in the supporting information section (Tables S1, S2 and S3). Hence, docking studies demonstrates the binding specificity of each compound for its interacting protein supporting the hypothesis that heteroaryl fragments might help to identify target specific or dual inhibitors.

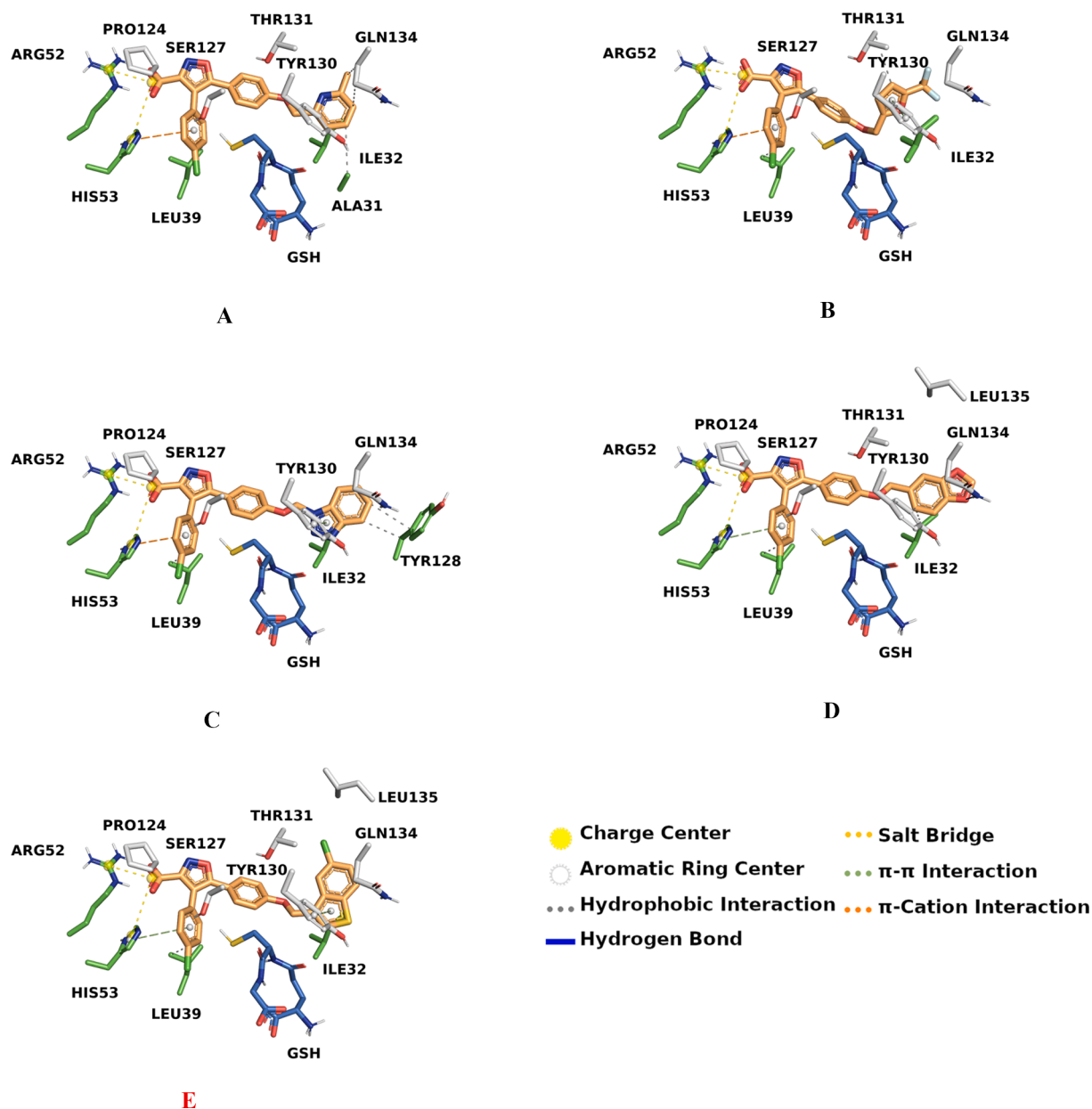


Fig. 3. Three-dimensional model of interactions of **17** (A), **18** (B), **19** (C), **25** (D), and **26** (E) with the mPGES-1 (PDB code 5TL9) binding site. Sticks in orange represents ligand, white represents chain 1, green represents chain 2, blue represents GSH. Legend of protein – ligand interactions as identified by *PLIP 1.4.4* [39] and visualized with *PyMOL 2.3* [40] (For interpretation of the references to color in this figure legend, the reader is referred to the web version of this article.)

2.3.2. Molecular dynamic studies

Since compound **18** with 5-CF₃-furan side arm demonstrated noteworthy dual inhibitor potency for both mPGES-1 (IC₅₀ = 0.16 μM) and 5-LO (IC₅₀ = 0.39 μM), the binding interactions of **18** with both proteins were further evaluated by molecular dynamic (MD) simulations (100 ns) to take into account potential ligand-induced conformational changes. Since the available mPGES-1 x-ray structure (PDB code 5TL9 [36]) does not include membrane coordinates, we analyzed the binding modes of mPGES-1/**18** complex by means of MD simulations by including membrane (taken from OPM Database [41]) in the simulation systems. By inclusion of the membrane bilayer, it was possible to observe the membrane's effect on the binding in which the adopted techniques have been widely used for the analysis of other membrane-embedded proteins. We used the human 5-LO crystal structure (PDB code 3O8Y [37]), for rationalizing the inhibitory activity of **18** by means of molecular docking and MD simulations to 5-LO. We combined docking studies with four copies of MD simulations to investigate the binding modes of **18**

considering ligand-induced conformational changes of mPGES-1 and 5-LO. Each copy of the molecular simulation showed similar interactions during the simulations (Fig. 6). The rationalization of the 5-LO binding mode was obtained considering the fundamental amino acids in the active site of both enzymes as described previously [24,42–44].

The results indicate that the interaction network obtained by 100 ns of MD simulations with four copies revealed new important interactions, which can unveil the potency of **18**. Some of the interactions, which were observed in docking simulations, were not maintained (<10%), and some additional interactions were observed during the simulations. As a result of MD studies, we observe that **18** perfectly fits into the active sites of both proteins. However, compared to the docking results, the ionic contacts with HIS53 of mPGES-1 and HIS600 of 5-LO are not maintained, and the carboxyl group is stabilized by ionic interactions with ARG52 of mPGES-1 and ASN425 of 5-LO as well as water-mediated hydrogen bonding with ARG52 and SER127 of mPGES-1 and TYR181, ALA424 and TRP599 of 5-LO (Fig. 7, Table 3). In addition, the formation

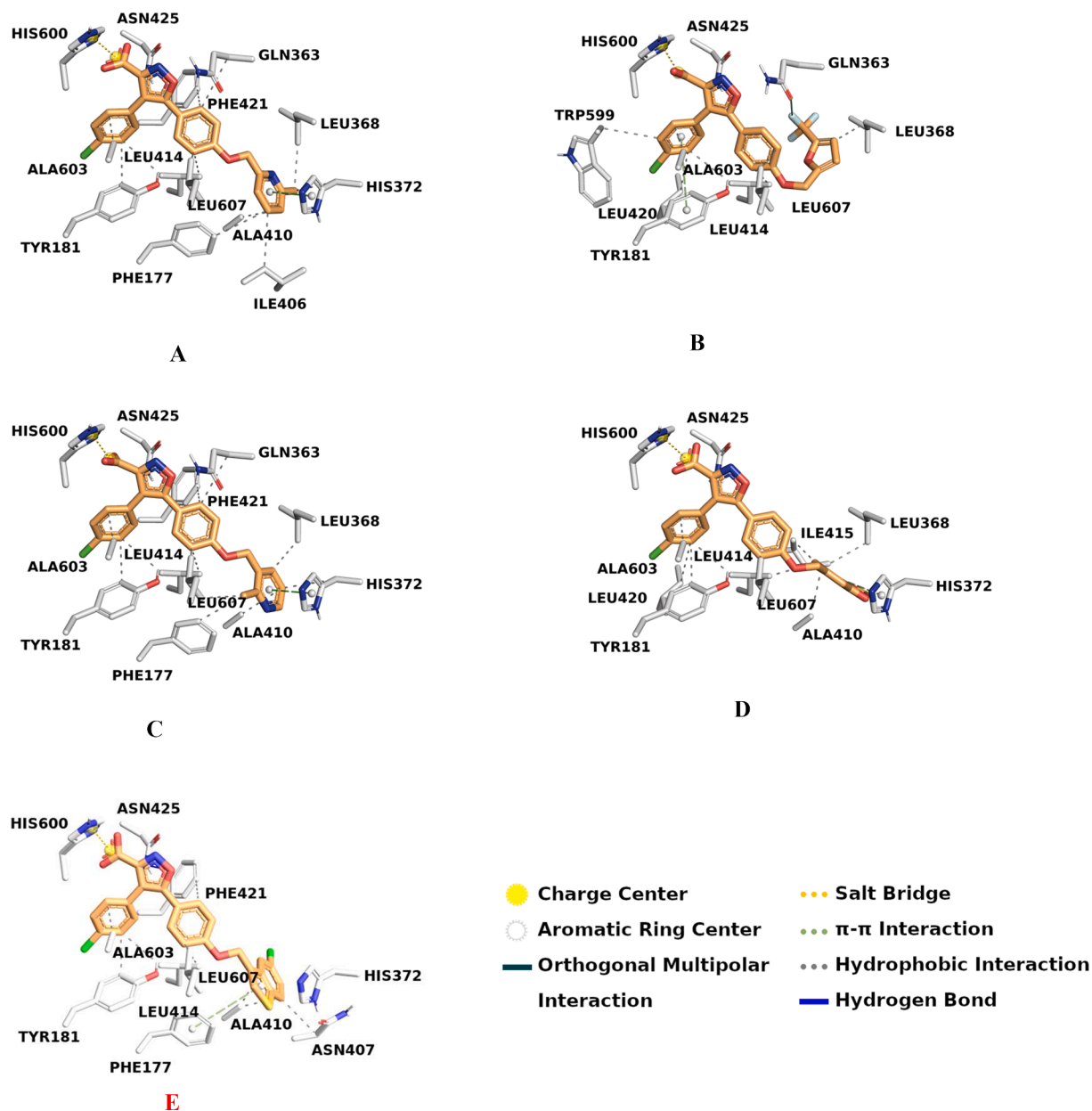


Fig. 4. Three-dimensional model of interactions of **17** (A), **18** (B), **24** (C), **25** (D), and **26** (E) with the 5-LO (PDB code 3O8Y) binding site. Sticks in orange represents ligand, white represents residues in chain 1. Legend of protein – ligand interactions as identified by *PLIP 1.4.4* [39] and visualized with *PyMOL 2.3* [40] (For interpretation of the references to color in this figure legend, the reader is referred to the web version of this article.)

of π - π interactions of 5-CF₃-furan with TYR130 of mPGES-1, and HIS367 and HIS372 of 5-LO along with hydrogen bonds with THR364, ARG411 and orthogonal multipolar interactions with ASN407 and ALA410 residues clearly help to stabilize **18** at the active site of both proteins. Moreover, *p*-chlorophenyl fits to the hydrophobic groove by making additional hydrophobic contacts with TYR130 of mPGES-1 and TYR181 of 5-LO, which is a gatekeeper amino acid along with PHE177 at the active site entrance of 5-LO. All the observed interactions with the occupancy values equal or higher than 10% were shown in the MD interaction figures (Fig. 7) and summarized in Table 3.

2.4. *In vivo* efficacy of compound **18** in animal model of inflammation

In view of the high potency of **18** for suppression of both PGE₂ and LT biosynthesis, we attempted to evaluate the anti-inflammatory effectiveness *in vivo* in the carrageenan-induced hind paw edema model in mice [45]. The carrageenan-induced paw edema is a well-known acute

model of inflammation that is widely used for screening novel anti-inflammatory compounds. The inflammatory response is usually quantified by an increase in paw size (edema) which is maximal around 5 h post-carrageenan injection and is known to be modulated by specific inhibitors of the AA inflammatory cascade. The results demonstrate that a significant reduction of paw edema from 90 to 360 min as compared to control group was observed in animals dosed with both the dual mPGES-1/5-LO inhibitor **18** (10 and 30 mg/kg) and the non-selective COX inhibitor indomethacin (10 mg/kg) used as reference control (Fig. 8). These results indicate that the anti-inflammatory effectiveness of **18** was comparable or even superior over the reference indomethacin. Moreover, **18** was further investigated for gastric toxicity upon acute administration to determine the ulcerogenic potential at the time interval in which the compound showed the highest anti-inflammatory activity (270 min). At doses of 10 and 30 mg/kg, **18** caused weak damage to the gastric mucosa (ratio of ulceration; control (DMSO and saline) 0/6; Indo 4/6 at 10 mg/kg; **18** 1/6 at 10 mg/kg, and 2/6 at 30

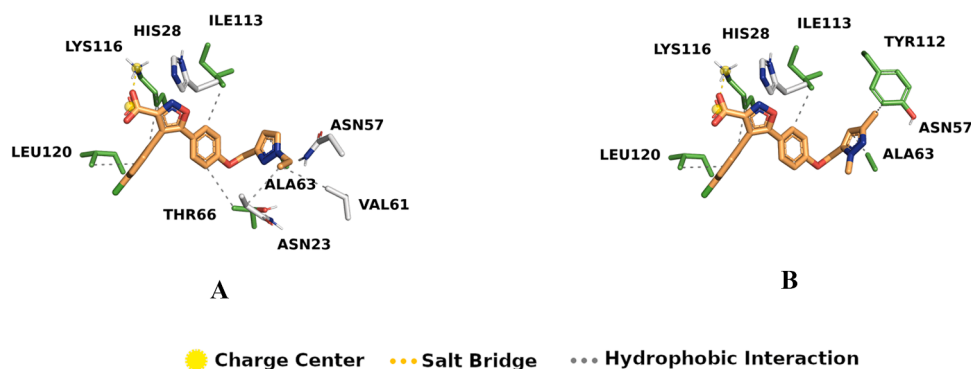


Fig. 5. Three-dimensional model of interactions of 21 (A), and 22 (B) with the FLAP (PDB code 2Q7M) binding site. Sticks in orange represents ligand, white represents residues in chain 1, green represents residues in chain 2. Legend of protein – ligand interactions as identified by *PLIP 1.4.4* [39] and visualized with *PyMOL 2.3* [40] (For interpretation of the references to color in this figure legend, the reader is referred to the web version of this article.)

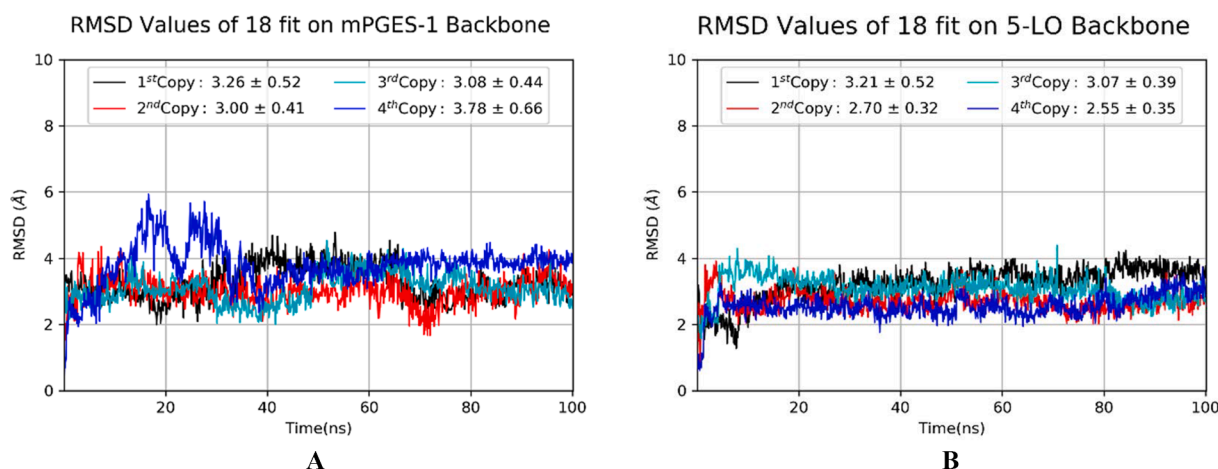


Fig. 6. Root-mean-square deviation (RMSD) values of 100 ns MD simulations of compound 18 fit to mPGES-1 (A) and 5-LO (B) backbone (each color presents one copy of the simulation).

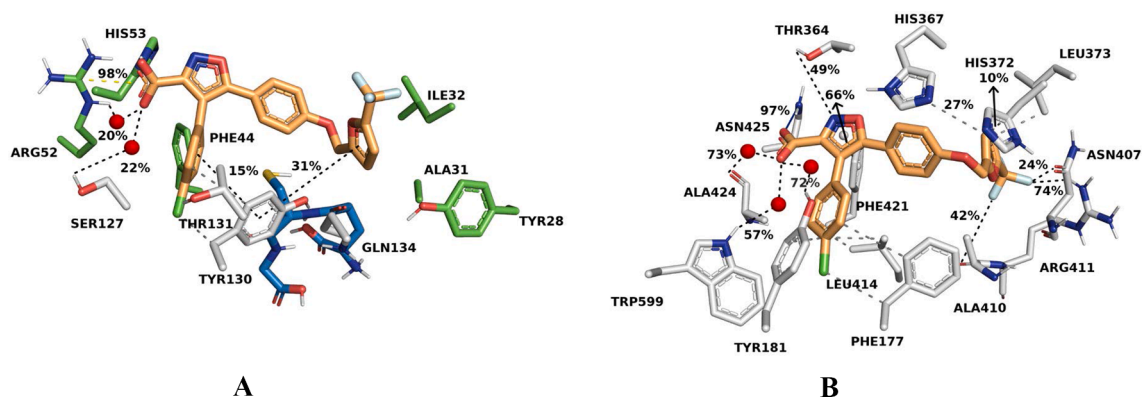


Fig. 7. Binding mode analysis of compound 18 during interaction with mPGES-1 (A, PDB code 5TL9) and 5-LO (B, PDB code 3O8Y). Main interactions are represented schematically with their occupancies calculated in the time window 0–100 ns. Sticks in orange represents ligand, white represents residues in chain 1, green represents residues in chain 2, blue represents GSH. Red spheres represent bridging water molecules. Interaction types are given in Table 3 to obtain a clearer view. (For interpretation of the references to color in this figure legend, the reader is referred to the web version of this article.)

mg/kg).

3. Conclusions

We have applied a convenient strategy for the synthesis of a small set of 4,5-diarylisoxazol-3-carboxylic acids for exploring the role of the heteroaryl fragments on the activity switch among closely related

biological targets within the AA cascade, namely mPGES-1, FLAP and 5-LO. In view of the good congruity between the results from the biological assays and the prediction of the molecular docking calculations, a satisfactory explanation of the putative binding modes in three protein targets for the 4,5-diarylisoxazol-3-carboxylic acid-based compounds was provided. Biological assays disclosed that the decorations on the heteroaryl side arm direct the activity against mPGES-1, FLAP and 5-LO,

Table 3

MD-based common interaction analysis of **18** with mPGES-1 and 5-LO. The occupancy values of vdW interactions were not calculated (n.c.), because of the additional contribution of several atoms that exist in the nature of the interaction type.

Fragment	Target		Occupancy		Interaction Type
	mPGES-1	Occupancy	5-LO	Occupancy	
Carboxylate Hydrophilic P.	ARG52	98%	ASN425	98%	Salt Bridge
	ARG52	20%	ALA424	73%	Water Bridge
	SER127	22%	TYR181	72%	
<i>p</i> -chlorophenyl Hydrophobic-1P.	LEU39	n.c.	TRP599	57%	
			TYR181	n.c.	vdW Interaction
			LEU414		
			ALA603		
Isoxazole-5-phenyl Hydrophobic-2P.	TYR130	15%	GLN363	n.c.	$\pi - \pi$ Stacking
	Membrane	n.c.			vdW Interaction
Heteroaryl Hydrophobic-3P.	ILE32	n.c.	PHE421	66%	$\pi - \pi$ Stacking
			THR364	49%	Hydrogen Bond
	GLN134	n.c.	LEU368	n.c.	vdW Interaction
	TYR130	31%	HIS372		
			HIS367	27%	$\pi - \pi$ Stacking
			HIS372	10%	
			ASN407	24%	Orthogonal Multipolar Interaction
ALA410			42%		
		ARG411	74%	Hydrogen Bond	

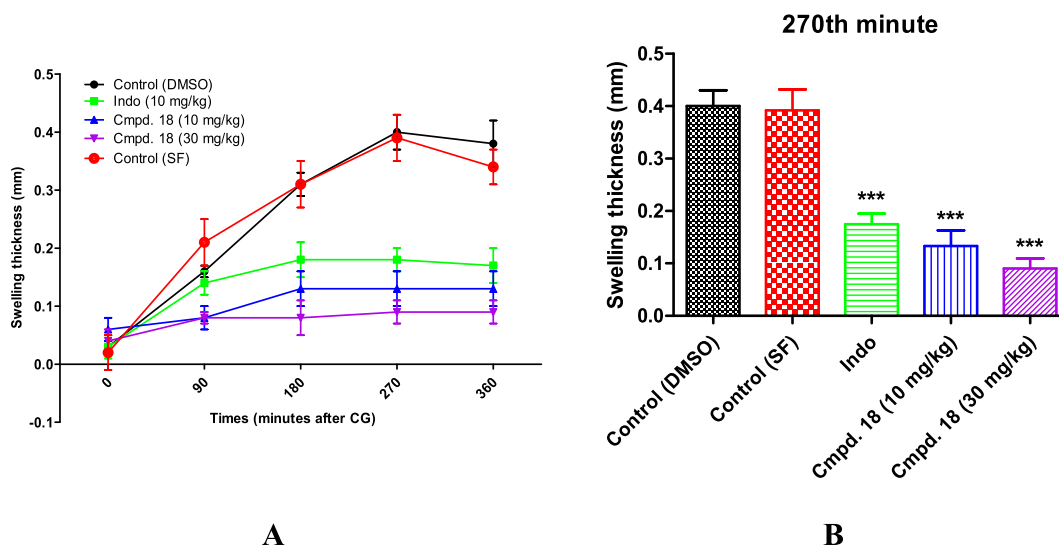


Fig. 8. A) Time-base scale of carrageenan-induced paw edema in 90, 180, 270, and 360 min. Values are expressed as mean \pm S.E.M. B) Effect of **18** on the carrageenan-induced paw edema of mice at 270th min. Values are expressed as mean \pm S.E.M. Differences from control, *** $P < 0.001$; SF, serum physiologic solution.

and have the potential to provide multitarget inhibitors, exemplified by compound **18**, with potent *in vitro* and *in vivo* efficacy. As future perspective, further investigations on the nature of the heteroaryl fragment can be fundamental to increase the interaction efficiency with the hydrophobic binding pocket of the active site in three target proteins to identify multitarget inhibitors. In conclusion, our results provide the efficiency of the heteroaryl side arm in the design of promising candidates as anti-inflammatory agents, and shed light on the chemical decorations functional for the design of further members belonging to this inhibitor class.

4. Experimental

4.1. Chemistry

Starting materials were purchased from commercial suppliers, and

used without further purification. ^1H and ^{13}C NMR spectra were recorded in CDCl_3 or $\text{DMSO}-d_6$ on a Varian Mercury 400 MHz spectrometer using tetramethylsilane as the internal standard. All chemical shifts were recorded as δ (ppm). All coupling constants are reported as Hertz. High resolution mass spectra data (HRMS) were collected using Waters LCT Premier XE Mass Spectrometer (high sensitivity orthogonal acceleration time-of-flight instrument) operating in ESI (+) or ESI (-) method, also coupled to an AQUITY Ultra Performance Liquid Chromatography system (Waters Corporation) using a UV detector monitoring at 254 nm. Purity for all final compounds were $> 95\%$, according to the UPLC-MS method using (A) water + 0.1% Formic Acid and (B) acetonitrile + 0.1% Formic Acid; flow rate = 0.3 ml/min, Column: Aquity BEH C18 column (2.1 \times 100 mm, 1.7 mm). The reactions were followed by TLC on precoated Merck silica gel plates purchased from Merck. The developed plates were visualized using 254 nm or 365 nm UV. Flash column chromatography on silica gel was performed on Interchim prepacked

disposable silica gel columns using Interchim Puriflash 4250 (Montluçon, France). Melting points of the synthesized compounds were determined by an SMP50 automatic melting point apparatus (Stuart, Staffordshire, ST15 OSA, UK) and were uncorrected. Compounds 1–6 were synthesized in the same manner as reported previously [24].

4.1.1. Synthesis of title isoxazol-3-carboxylic acid derivatives 17–26

Ester intermediates 7–16 (0.004 mol) and lithium hydroxide (0.008 mol) in THF/water mixture (1:1) were stirred at 60 °C for 2 h. After the reaction is complete, the reaction mixture was allowed to cool to ambient temperature, diluted with water, acidified with 2 N HCl to pH 6, and the resulting precipitate was filtered and recrystallized from the appropriate solvent or purified by automated flash chromatography.

4.1.1.1. 4-(4-Chlorophenyl)-5-{4-[(6-methylpyridin-2-yl)methoxy]phenyl}isoxazole-3-carboxylic acid (17). Purified by recrystallization from ethyl acetate. Yield 34%; mp 193.7–195.1 °C. ¹H NMR (DMSO-*d*₆): δ 2.46 (3H, s), 5.12 (2H, s), 6.90 (2H, d, *J* = 8.4 Hz), 7.09 (2H, d, *J* = 8.4 Hz), 7.17 (1H, d, *J* = 7.6 Hz), 7.29 (1H, d, *J* = 7.6 Hz), 7.51 (2H, d, *J* = 8.0 Hz), 7.69 (1H, t, *J* = 7.6 Hz), 7.98 (2H, d, *J* = 8.0 Hz); ¹³C NMR (DMSO-*d*₆): δ 23.9, 70.2, 113.1, 115.2, 118.5, 122.1, 123.3, 124.4, 126.9, 128.2, 129.1, 131.4, 137.1, 137.9, 139.8, 156.1, 157.4, 157.8, 180.1; HRMS *m/z* [M + H]⁺ calcd for C₂₃H₁₈ClN₂O₄ 421.0955; found 421.0965.

4.1.1.2. 4-(4-Chlorophenyl)-5-{4-[(5-(trifluoromethyl)furan-2-yl)methoxy]phenyl}isoxazole-3-carboxylic acid (18). Purified by successive washing with hot hexane. Yield 73%; mp 133.8–135.8 °C. ¹H NMR (DMSO-*d*₆): δ 5.18 (2H, s), 6.82 (1H, d, *J* = 3.6 Hz), 7.09 (2H, d, *J* = 8.8 Hz), 7.19–7.20 (1H, m), 7.34–7.39 (4H, m), 7.44 (2H, d, *J* = 8.8 Hz); ¹³C NMR (DMSO-*d*₆, NaH): δ 61.5, 73.4, 112.0, 113.6, 114.3 (³*J*_{C-F} = 2.3 Hz), 119.4 (¹*J*_{C-F} = 265.2 Hz), 124.3, 124.6, 125.1, 127.5, 129.1, 129.6, 138.5, 139.7, 140.6 (²*J*_{C-F} = 41.2 Hz), 154.2, 157.7, 182.4; HRMS (*m/z*): [M + H]⁺ calcd for C₂₂H₁₄ClF₃NO₅ 464.0513; found 464.0504.

4.1.1.3. 5-{4-[(1H-1,2,3-Benzotriazol-1-yl)methoxy]phenyl}-4-(4-chlorophenyl)isoxazole-3-carboxylic acid (19). Purified by recrystallization from methanol. Yield 88%; mp 173.6–174.9 °C. ¹H NMR (DMSO-*d*₆): δ 6.82 (2H, s), 7.24 (2H, d, *J* = 8.8 Hz), 7.36–7.46 (5H, m), 7.48 (2H, d, *J* = 8.8 Hz), 7.62 (1H, t, *J* = 7.6 Hz), 7.95 (1H, d, *J* = 8.4 Hz), 8.09 (1H, d, *J* = 8.4 Hz); ¹³C NMR (DMSO-*d*₆): δ 73.5, 110.6, 114.3, 116.5, 119.4, 120.5, 124.7, 127.9, 128.3, 128.5, 128.6, 132.0, 132.6, 133.1, 145.3, 155.9, 157.5, 160.7, 166.0; HRMS *m/z* [M + H]⁺ calcd for C₂₃H₁₆ClN₄O₄ 447.0860; found 447.0860.

4.1.1.4. 4-(4-Chlorophenyl)-5-{4-[(1-propyl-1H-imidazo[4,5-c]pyridin-2-yl)methoxy]phenyl}isoxazol-3-carboxylic acid (20). Purified by recrystallization from methanol. Yield 83%; mp 148.7–150.3 °C. ¹H NMR (DMSO-*d*₆): δ 0.86 (3H, t, *J* = 7.2 Hz), 1.77–1.82 (2H, m), 4.29 (2H, t, *J* = 7.2 Hz), 5.51 (2H, s), 7.18 (2H, d, *J* = 8.4 Hz), 7.38 (2H, d, *J* = 8.0 Hz), 7.42 (2H, d, *J* = 8.4 Hz), 7.48 (2H, d, *J* = 8.0 Hz), 7.76 (1H, d, *J* = 4.8 Hz), 8.39 (1H, d, *J* = 4.8 Hz), 9.0 (1H, s); ¹³C NMR (DMSO-*d*₆): δ 10.9, 22.6, 45.3, 62.3, 106.6, 113.9, 115.4, 119.6, 128.2, 128.4, 128.5, 131.9, 133.0, 139.0, 140.5, 140.7, 141.1, 151.3, 156.3, 159.2, 160.8, 166.0; HRMS *m/z* [M + H]⁺ calcd for C₂₆H₂₂ClN₄O₄ 489.1330; found 489.1308.

4.1.1.5. 4-(4-Chlorophenyl)-5-{4-[(1-ethyl-1H-pyrazol-3-yl)methoxy]phenyl}isoxazole-3-carboxylic acid (21). Purified by recrystallization from hexane-ethyl acetate. Yield 45%; mp 189.6–190.8 °C. ¹H NMR (DMSO-*d*₆): δ 1.33 (3H, t, *J* = 7.2 Hz), 4.08 (2H, q, *J* = 7.2 Hz), 5.00 (2H, s), 6.27 (1H, d, *J* = 2.0 Hz), 7.06 (2H, d, *J* = 8.8 Hz), 7.36 (2H, d, *J* = 8.8 Hz), 7.37 (2H, d, *J* = 8.8 Hz), 7.48 (2H, d, *J* = 8.8 Hz), 7.67 (1H, d, *J* = 2.0 Hz); ¹³C NMR (DMSO-*d*₆): δ 15.4, 46.1, 63.8, 105.1, 113.8, 115.3, 118.7, 128.2, 128.3, 128.6, 130.2, 132.0, 133.1, 146.4, 155.9, 160.0,

160.8, 166.4; HRMS *m/z* [M + H]⁺ calcd for C₂₂H₁₉ClN₃O₄ 424.1064; found 424.1074.

4.1.1.6. 4-(4-Chlorophenyl)-5-{4-[(1,3-dimethyl-1H-pyrazol-5-yl)methoxy]phenyl}isoxazole-3-carboxylic acid (22). Purified by recrystallization from methanol. Yield 72%; mp 190.7–192.3 °C. ¹H NMR (DMSO-*d*₆): δ 2.08 (3H, s), 3.70 (3H, s), 5.11 (2H, s), 6.12 (1H, s), 7.08 (2H, d, *J* = 8.8 Hz), 7.36 (2H, d, *J* = 8.8 Hz), 7.38 (2H, d, *J* = 8.8 Hz), 7.48 (2H, d, *J* = 8.8 Hz); ¹³C NMR (DMSO-*d*₆): δ 13.1, 36.0, 60.1, 106.5, 113.9, 115.4, 119.1, 128.1, 128.4, 128.6, 132.0, 133.1, 137.4, 145.6, 155.9, 159.5, 160.8, 166.3; HRMS *m/z* [M + H]⁺ calcd for C₂₂H₁₉ClN₃O₄ 424.1064; found 424.1061.

4.1.1.7. 4-(4-Chlorophenyl)-5-{4-[(1-(propan-2-yl)-1H-imidazol-2-yl)methoxy]phenyl}isoxazole-3-carboxylic acid (23). Purified by recrystallization from methanol. Yield 95%; mp 126.4–127.7 °C. ¹H NMR (DMSO-*d*₆): δ 1.37 (6H, d, *J* = 6.4 Hz), 4.52–4.59 (1H, m), 5.27 (2H, s), 7.11 (1H, s), 7.14 (2H, d, *J* = 8.8 Hz), 7.37 (2H, d, *J* = 8.4 Hz), 7.39 (2H, d, *J* = 8.8 Hz), 7.48 (2H, d, *J* = 8.4 Hz), 7.53 (1H, s); ¹³C NMR (DMSO-*d*₆): δ 23.1, 48.1, 61.1, 113.8, 115.4, 118.2, 119.5, 125.7, 128.2, 128.4, 128.6, 132.0, 133.0, 141.0, 156.6, 159.3, 161.0, 165.9; HRMS *m/z* [M + H]⁺ calcd for C₂₃H₂₁ClN₃O₄ 438.1221; found 438.1200.

4.1.1.8. 4-(4-Chlorophenyl)-5-{4-[(2-methylpyridin-3-yl)methoxy]phenyl}isoxazole-3-carboxylic acid (24). Purified by recrystallization from methanol. Yield 45%; mp 154.3–155.9 °C. ¹H NMR (DMSO-*d*₆): δ 2.50 (3H, s), 5.16 (2H, s), 7.01 (2H, d, *J* = 8.4 Hz), 7.18 (2H, d, *J* = 8.4 Hz), 7.23–7.27 (1H, m), 7.56 (2H, d, *J* = 7.8 Hz), 7.79–7.82 (1H, m), 7.94 (2H, d, *J* = 7.8 Hz), 8.40–8.42 (1H, m); ¹³C NMR (DMSO-*d*₆): δ 22.2, 67.4, 113.9, 115.1, 121.7, 124.7, 124.9, 125.6, 127.7, 129.9, 130.8, 131.8, 136.2, 137.0, 139.1, 148.6, 157.2, 158.6, 179.9; HRMS *m/z* [M + H]⁺ calcd for C₂₃H₁₈ClN₂O₄ 421.0955; found 421.0938.

4.1.1.9. 5-{4-[(2H-1,3-Benzodioxol-5-yl)methoxy]phenyl}-4-(4-chlorophenyl)-1,2-oxazole-3-carboxylic acid (25). Purified by recrystallization from methanol. Yield 69%; mp 167.7–168.2 °C. ¹H NMR (DMSO-*d*₆): δ 4.99 (2H, s), 6.01 (2H, s), 6.88–6.93 (2H, m), 6.99 (1H, s), 7.05 (2H, d, *J* = 8.4 Hz), 7.37 (4H, d, *J* = 8.4 Hz), 7.48 (2H, d, *J* = 8.4 Hz); ¹³C NMR (DMSO-*d*₆): δ 69.2, 100.9, 108.1, 108.5, 113.5, 115.3, 118.8, 121.7, 122.1, 128.3, 128.5, 130.0, 131.9, 132.9, 146.9, 147.3, 156.6, 159.9, 160.9, 165.9; HRMS *m/z* [M + H]⁺ calcd for C₂₄H₁₇ClNO₆ 450.0744; found 450.0741.

4.1.1.10. 5-{4-[(5-Chloro-1-benzothiophen-3-yl)methoxy]phenyl}-4-(4-chlorophenyl)-1,2-oxazole-3-carboxylic acid (26). Purified by recrystallization from methanol. Yield 44%; mp 170.8–171.7 °C. ¹H NMR (DMSO-*d*₆): δ 5.38 (2H, s), 7.15 (2H, d, *J* = 8.8 Hz), 7.37–7.44 (5H, m), 7.49 (2H, d, *J* = 8.4 Hz), 7.94 (2H, d, *J* = 2.0 Hz), 7.97 (1H, s), 8.04 (1H, d, *J* = 8.4 Hz); ¹³C NMR (DMSO-*d*₆): δ 63.8, 113.8, 115.4, 118.9, 121.6, 124.5, 124.6, 128.1, 128.3, 128.6, 129.0, 129.5, 130.8, 132.0, 133.0, 138.3, 138.9, 155.9, 159.8, 160.7, 166.3; HRMS *m/z* [M + H]⁺ calcd for C₂₅H₁₆Cl₂NO₄S 496.0177; found 496.0170.

4.2. Computational methods

4.2.1. Molecular docking studies

The probable binding orientations of the active compounds were identified by conducting molecular docking studies against mPGES-1, 5-LO and FLAP by following the previously applied procedures [24,42–44]. The PDB codes of the crystal structures used in this study are 5TL9 [36], 3O8Y [37] and 2Q7M [38], respectively. The docking results of 17, 18, 19, 25, 26 were visualized at the mPGES-1 active site, 17, 18, 24, 25, 26 were visualized at the 5-LO active site, and 17, 18, 21, 22, 24, 25, 26 were visualized at FLAP active site.

Crystal selection was made (i) from the crystals that contain

glutathione (GSH) and a potent mPGES-1 inhibitor in the active site of the complex, (ii) having a better crystal resolution, (iii) being co-crystallized with potent mPGES-1 inhibitors, (iv) analysis of electron density maps and (v) reproducibility of the ligand binding mode of the co-crystallized ligand by the applied docking protocol for mPGES-1. Regarding crystal selection for 5-LO, the selected structure is found suitable for docking 4,5-diarylisoazol-3-carboxylic acid derivatives. The other ones either (i) include a mutated residue to mimic 15-LO's or a natural product which is identified (ii) a redox inhibitor or (iii) an allosteric inhibitor. Selected FLAP crystal structure is obtained in low-resolution, however we used a refined model of the original structure by applying a relaxation protocol. The readers are invited to read further our previous publication for further details [23]. The relaxed FLAP model is compared with recently published crystals and low RMSD value is obtained (RMSD < 0.5) by aligning the displayed active site residues in Fig. 5. A brief report of each published crystal structure is given in Table S4, S5 and S6.

Ligands were drawn by using *Maestro 11.1* [46] Interface. The atom types and the protonation states of the proteins and the ligands were identified with OPLS2005 forcefield. *Protein Preparation Wizard* [47] was used to parameterize the atom types, to add predicted positions of the missing side chains, and to relax the active sites of the proteins. *LigPrep* [48] routine was used at pH 7.0 ± 2.0 to prepare the ligands.

The predicted protein-ligand interactions by docking studies were generated with *Glide 7.4* [49–51]. Firstly, the docking boxes were generated by identifying binding sites' centroids with the amino acid residues that are present in docking figures. These centroids' coordinates were used to identify binding site enclosing boxes and to limit each docked pose's distance to this point by 10 Å. Van der Waals radius scaling factor and partial charge cutoff values are kept with their default values (1.0 and 0.25, respectively). The docking simulations were done in standard precision mode (GlideScore SP) [49,51,52]. The most representative binding mode of 4,5-diarylisoazol-3-carboxylic acid derivatives for each target were identified by (i) keeping top 5 ranked poses by their docking scores and (ii) selecting the lowest RMSD value one for each ligand within all docked poses. Image generation was done with PyMOL 2.3 [40] after identifying protein-ligand contacts with PLIP 1.4.4 [39]. Directional and non-directional interactions are identified by PLIP 1.4.4's [39] rule-based detection algorithm [53] with default parameters [54] to visualize the interactions. Hydrophilic interactions are identified based on their distance and angle cutoffs [54]. However, hydrophobic interactions are a result from their entropic effects, therefore there are no clear geometries for their association. We stored these occurrences in static pictures by using the generous cutoffs of PLIP 1.4.4 [39]. Salt bridges are identified by the identification of opposite charged atoms and then controlling the distances between to be below 5.5 Å [55]. π - π interactions are identified by computationally placing dummy atoms to the middle of the appropriate rings' centers and checking formation of parallel or T shaped π -stackings by their distances or angles [56]. Van der Waals interactions were identified similarly. Firstly, carbon atoms that are bound to other carbons or hydrogens are classified as hydrophobic atom, then distances between such atoms are analyzed and close ones are identified as interacting atoms. Only the closest ones within these residues are shown as interaction for a clear visualization. Further information can be found in the source code [53,54].

4.2.2. Molecular dynamic (MD) studies

The best ranking docking result of compound **18** with mPGES-1 and 5-LO were used to evaluate the predicted binding modes further. The simulation systems were generated with *System Builder* utility, to run MD simulations with *Desmond 4.9* [57]. mPGES-1 complex including **18** was embedded in dipalmitoyl phosphatidylcholine (DPPC) bilayers to include membrane structure in the simulation system. The predicted location of the lipid bilayer was obtained from Orientations of Proteins in Membrane (OPM) [41] database. SPC model was used for water molecules. Recording interval is set to 10 picoseconds while saving the

MD trajectories and energy calculation results for each trajectory. The simulation system relaxation protocol is given in as stages before starting the main MD simulation. There were 9335 water molecules for mPGES-1 simulation and 22,988 water molecules for 5-LO. Long-range Coulombic interactions cutoff radius value was set to 9.0 Å. All the simulation systems were prepared with OPLS2005 forcefield. The systems were neutralized, and the salt concentrations were defined as 0.15 M, and calculated numbers of Na^+ and Cl^- ions were added. The simulations were started to run with the relaxation protocol of a series of standard minimization and short MD simulations to relax the systems. The relaxation protocol is applied as described followingly. Initial system relaxations were conducted with up to 2000 minimization steps, a convergence criterion of 50 kcal/mol/Å, and the presence of harmonic restraints on the solute atoms (force constant = 50.0 kcal/mol/Å²). In the second step, minimization routines were conducted without restraints. The third stage includes 12 ps at 10 K with harmonic restraints on the heavy atoms of the solute (force constant = 50.0 kcal/mol/Å²), by using NVT ensemble and Berendsen thermostat. The fourth step 12 ps at 10 K, by retaining the harmonic restraints and using NPT ensemble and Berendsen thermostat and barostat. The fifth step was done to heat the system for 24 ps at 323 K (above the transition temperature (314.4 K) of DPPC from gel to liquid [58]), by retaining the harmonic restraints and using NPT ensemble and Berendsen thermostat and barostat. At the final stage of the relaxation of the system was done for 24 ps at 323 K without harmonic restraints, by using NPT ensemble and Nose-Hoover thermostat and Martyna-Tobias-Klein barostat. Subsequently, 100 ns long MD simulations were carried out with four copies for both simulation systems, to have statistically more reliable results. All the simulations were run with an NPT ensemble at 323 K. The simulation trajectories were visualized with *Maestro 11.1* [46] and *VMD 1.9.3* [59]. The protein-ligand interaction occupancy values and RMSD values during the simulations were evaluated with *Simulation Interactions Diagram* module, and further interaction analyses of trifluoromethyl moiety of **18** were done with *Simulation Event Analysis* module of *Schrodinger Suite 2017-1*. Conformational clustering was done with *gmx cluster* module of *GROMACS 2018.3* [60] with a cut-off value of 0.5 Å to obtain the most representative snapshot from the whole 100 ns simulation. Later, the pose generations on the highest populated pose for each protein was done with *PLIP 1.4.4* [39] and *PyMOL 2.3* [40].

4.3. Biological assays

4.3.1. Cells

Neutrophils were isolated from human blood as reported before [25]. Briefly, human peripheral blood was obtained from healthy adult (18–65 years) male and female donors with consent that had not taken antiinflammatory drugs during the last 10 days, by venipuncture in heparinized tubes (16 IE heparin/ml blood; University Hospital Jena, Germany). The blood was centrifuged (4000 × g for 20 min at 20 °C) for preparation of leukocyte concentrates. Leukocyte concentrates were then subjected to dextran sedimentation and centrifugation on Nycoprep cushions. Contaminating erythrocytes of pelleted neutrophils were lysed by hypotonic lysis using water. Neutrophils were washed twice in ice-cold PBS (purity > 96–97%) and finally resuspended in PBS pH 7.4 containing 1 mg/ml glucose and 1 mM CaCl_2 (PGC buffer). For analysis of acute cytotoxicity of the compounds during preincubation periods (30 min at 37 °C), cellular integrity of neutrophils was analyzed by trypan blue exclusion with a Vi-cell counter (Beckmann Coulter GmbH, Krefeld). None of the compounds caused significant loss of neutrophil viability within 30 min (studied by trypan blue staining and light microscopy, data not shown).

4.3.2. Determination of 5-LO products in intact cells

For determination of LO products in intact cells, neutrophils (5×10^6) were resuspended in 1 ml PGC buffer, preincubated for 15 min at 37 °C with test compounds or vehicle (0.1% DMSO) and Ca^{2+} -ionophore

A23187 (2.5 mM) was added. After 10 min at 37 °C, the reaction was stopped on ice by addition of 1 ml of methanol. 30 µl 1 N HCl and 500 µl PBS, and 200 ng prostaglandin (PG)_{B1} were added and the samples were subjected to solid phase extraction on C18-columns (100 mg, UCT, Bristol, PA, USA). 5-LO products (LTB₄ and its *trans*-isomers, and 5-H(P)ETE) were analyzed by RP-HPLC and quantities calculated on the basis of the internal standard PGB₁. Cys-LTs C₄, D₄ and E₄ were not detected (amounts were below detection limit), and oxidation products of LTB₄ were not determined.

4.3.3. Determination of the activity of isolated 5-LO in cell-free assays

Escherichia coli BL21 cells were transformed with pT3-5-LO plasmid, and recombinant 5-LO protein was expressed at 27 °C as described [25]. Cells, resuspended in 50 mM triethanolamine/HCl pH 8.0, 5 mM EDTA, soybean trypsin inhibitor (60 µg/ml), 1 mM phenylmethanesulphonyl fluoride, and lysozyme (500 µg/ml), were homogenized by sonication (3 × 15 s). After centrifugation at 40,000g for 20 min at 4 °C, the supernatant was applied to an ATP-agarose column to partially purify 5-LO as described previously [21]. Aliquots of semi-purified 5-LO were diluted with ice-cold PBS containing 1 mM EDTA, and 1 mM ATP was added. Samples were pre-incubated with the test compounds or vehicle (0.1% DMSO) as indicated. After 15 min at 4 °C, samples were pre-warmed for 30 s at 37 °C, and 2 mM CaCl₂ plus 20 µM AA was added to initiate 5-LO product formation. After 10 min at 37 °C, the reaction was stopped by addition of 1 ml ice-cold methanol, and the formed metabolites were analyzed by RP-HPLC as described [21]. 5-LO products include the all-*trans* isomers of LTB₄ and 5-H(P)ETE.

4.3.4. Determination of mPGES-1 activity

Microsomal preparations of A549 cells expressing mPGES-1 were prepared as previously described [26]. In brief, A549 cells were cultivated in DMEM containing FCS (2%) and IL-1β (2 ng mL⁻¹) for 72 h (37 °C, 5% CO₂). Cells were harvested and resuspended in homogenization buffer consisting of potassium phosphate (0.1 M, pH 7.4), phenylmethanesulfonyl fluoride (1 mM), soybean trypsin inhibitor (60 µg mL⁻¹), leupeptin (1 µg mL⁻¹), glutathione (2.5 mM), and sucrose (250 mM). After shock-freezing of the cells in liquid nitrogen, sonication (3 × 20 s), and differential centrifugation at 10000 × g (10 min, 4 °C) and 174000g (60 min, 4 °C), the pellets were resuspended in homogenization buffer. Microsomes were diluted in potassium phosphate buffer (0.1 M, pH 7.4) with glutathione (2 mM) and pre-incubated with the test compounds or vehicle (0.1% DMSO) on ice for 15 min. After stimulation for 1 min at 4 °C with 20 µM PGH₂ as substrate, the reaction was terminated by the addition of stop solution containing FeCl₃ (40 mM), citric acid (80 mM), and 11β-PGE₂ (10 µM, as internal standard) and analyzed for PGE₂ by RP-HPLC as reported before [26].

4.4. Statistics

Results are presented as mean ± standard error of the mean (SEM) out of n independent experiments, where n represents the number of performed experiments on different days or with different donors. IC₅₀ values were calculated from at least 5 different concentrations using a nonlinear regression interpolation of semi-logarithmic graphs using GraphPad Prism (Graphpad Software Inc., San Diego, CA). Statistical evaluation was performed by one-way ANOVA using GraphPad InStat (Graphpad Software Inc., San Diego, CA) followed by a Bonferroni post-hoc test for multiple or student *t*-test for single comparisons, respectively. P-values < 0.05 were considered as significant.

CRediT authorship contribution statement

Tuğba Gürses: Investigation. **Abdurrahman Olğaç:** Investigation, Visualization. **Ulrike Garscha:** Methodology, Investigation. **Tuğçe Gür Maz:** Methodology, Formal analysis. **Nur Banu Bal:** Investigation. **Orhan Uludağ:** Methodology. **Burcu Çalışkan:** Supervision, Writing -

original draft. **Ulrich S. Schubert:** Resources. **Oliver Werz:** Resources, Supervision. **Erden Banoglu:** Conceptualization, Resources, Writing - review & editing, Funding acquisition.

Declaration of Competing Interest

The authors declare that they have no known competing financial interests or personal relationships that could have appeared to influence the work reported in this paper.

Acknowledgements

We acknowledge the Turkish Academy of Sciences (TUBA) for partial financial support. The GPUs used in this study were donated by NVIDIA Corporation. This work was also supported by the Deutsche Forschungsgemeinschaft, SFB1278/1 Polytarget 316213987 project A04.

Appendix A. Supplementary material

Supplementary data to this article can be found online at <https://doi.org/10.1016/j.bioorg.2021.104861>.

References

- [1] M.T. Donnelly, C.J. Hawkey, Review article: COX-II inhibitors—a new generation of safer NSAIDs? *Aliment. Pharmacol. Ther.* 11 (2) (1997) 227–236.
- [2] S. Tacconelli, A. Bruno, R. Grande, P. Ballerini, P. Patrignani, Nonsteroidal anti-inflammatory drugs and cardiovascular safety - translating pharmacological data into clinical readouts, *Expert Opin. Drug Saf.* 16 (7) (2017) 791–807.
- [3] H.H. Chang, E.J. Meuliet, Identification and development of mPGES-1 inhibitors: where we are at? *Future Med. Chem.* 3 (15) (2011) 1909–1934.
- [4] A. Koeberle, O. Werz, Perspective of microsomal prostaglandin E2 synthase-1 as drug target in inflammation-related disorders, *Biochem. Pharmacol.* 98 (1) (2015) 1–15.
- [5] A. Koeberle, O. Werz, Inhibitors of the microsomal prostaglandin E(2) synthase-1 as alternative to non steroidal anti-inflammatory drugs (NSAIDs)-a critical review, *Curr. Med. Chem.* 16 (32) (2009) 4274–4296.
- [6] D. Xu, S.E. Rowland, P. Clark, A. Giroux, B. Cote, S. Guiral, M. Salem, Y. Ducharme, R.W. Friesen, N. Methot, J. Mancini, L. Audoly, D. Riendeau, MF63 [2-(6-chloro-1H-phenanthro[9,10-d]imidazol-2-yl)-isophthalonitrile], a selective microsomal prostaglandin E synthase-1 inhibitor, relieves pyresis and pain in preclinical models of inflammation, *J. Pharmacol. Exp. Ther.* 326 (3) (2008) 754–763.
- [7] Y. Jin, C.L. Smith, L. Hu, K.M. Campanale, R. Stoltz, L.G. Huffman Jr., T. A. McNearney, X.Y. Yang, B.L. Ackermann, R. Dean, A. Regev, W. Landschulz, Pharmacodynamic comparison of LY3023703, a novel microsomal prostaglandin e synthase 1 inhibitor, with celecoxib, *Clin. Pharmacol. Ther.* 99 (3) (2016) 274–284.
- [8] B.H. Norman, M.J. Fisher, M.A. Schiffler, S.L. Kuklish, N.E. Hughes, B.A. Czeskis, K. C. Cassidy, T.L. Abraham, J.J. Alberts, D. Luffer-Atlas, Identification and mitigation of reactive metabolites of 2-aminoimidazole-containing microsomal prostaglandin E synthase-1 inhibitors terminated due to clinical drug-induced liver injury, *J. Med. Chem.* 61 (5) (2018) 2041–2051.
- [9] S. Sant, M. Tandon, V. Menon, G. Gudi, V. Kattige, N.K. Joshi, K. Korukonda, O. Levine-Dolberg, *Grc* 27864, novel, microsomal prostaglandin E synthase-1 enzyme inhibitor: Phase 1 study to evaluate safety, Pk and Biomarkers in Healthy, Adult Subjects, *Osteoarthr Cartilage* 26 (2018) S351–S352.
- [10] Z.T. Gur, B. Caliskan, E. Banoglu, Drug discovery approaches targeting 5-lipoxygenase-activating protein (FLAP) for inhibition of cellular leukotriene biosynthesis, *Eur. J. Med. Chem.* 153 (2018) 34–48.
- [11] O. Radmark, O. Werz, D. Steinhilber, B. Samuelsson, 5-Lipoxygenase, a key enzyme for leukotriene biosynthesis in health and disease, *Biochim Biophys Acta* 1851 (4) (2015) 331–339.
- [12] M. Lemurell, J. Ulander, S. Winiwarer, A. Dahlen, O. Davidsson, H. Emtenas, J. Broddefalk, M. Swanson, D. Hovdal, A.T. Plowright, A. Pettersen, M. Ryden-Landergren, J. Barilind, A. Llinas, M. Herslof, T. Drmot, K. Sigfridsson, S. Moses, C. Whatling, Discovery of AZD6642, an inhibitor of 5-lipoxygenase activating protein (FLAP) for the treatment of inflammatory diseases, *J. Med. Chem.* 58 (2) (2015) 897–911.
- [13] D. Pettersen, J. Broddefalk, H. Emtenas, M.A. Hayes, M. Lemurell, M. Swanson, J. Ulander, C. Whatling, C. Amilon, H. Ericsson, A. Westin Eriksson, K. Granberg, A.T. Plowright, I. Shamovsky, A. Dellsen, M. Sundqvist, M. Nagard, E.L. Lindstedt, Discovery and early clinical development of an inhibitor of 5-lipoxygenase activating protein (AZD5718) for treatment of coronary artery disease, *J. Med. Chem.* 62 (9) (2019) 4312–4324.
- [14] H. Takahashi, D. Riether, A. Bartolozzi, T. Bosanac, V. Berger, R. Binetti, J. Broadwater, Z. Chen, R. Crux, S. De Lombaert, R. Dave, J.A. Dines, T. Fadrah-Khan, A. Flegg, M. Garrigou, M.H. Hao, J. Huber, J.M. Hutzler, S. Kerr, A. Kotey, W. Liu, H.Y. Lo, P.L. Loke, P.E. Mahaney, T.M. Morwick, S. Napier, A. Olague, E. Pack, A.K. Padyana, D.S. Thomson, H. Tye, L. Wu, R.M. Zindell,

- A. Abeywardane, T. Simpson, Synthesis, SAR, and series evolution of novel oxadiazole-containing 5-lipoxygenase activating protein inhibitors: discovery of 2-[4-(3-((r)-1-[4-(2-amino-pyrimidin-5-yl)-phenyl]-1-cyclopropyl-ethyl)-[1,2,4]oxadiazol-5-yl)-pyrazol-1-yl]-N, N-dimethyl-acetamide (BI 665915), *J. Med. Chem.* 58 (4) (2015) 1669–1690.
- [15] F. Celotti, S. Laufer, Anti-inflammatory drugs: New multitarget compounds to face an old problem. The dual inhibition concept, *Pharmacol. Res.* 43 (5) (2001) 429–436.
- [16] S.K. Kulkarni, V.P. Singh, Licofelone: the answer to unmet needs in osteoarthritis therapy? *Curr. Rheumatol. Rep.* 10 (1) (2008) 43–48.
- [17] E. Banoglu, B. Caliskan, S. Luderer, G. Eren, Y. Ozkan, W. Altenhofen, C. Weinigel, D. Barz, J. Gerstmeier, C. Pergola, O. Werz, Identification of novel benzimidazole derivatives as inhibitors of leukotriene biosynthesis by virtual screening targeting 5-lipoxygenase-activating protein (FLAP), *Bioorg. Med. Chem.* 20 (12) (2012) 3728–3741.
- [18] B. Caliskan, E. Banoglu, Overview of recent drug discovery approaches for new generation leukotriene A4 hydrolase inhibitors, *Expert Opin. Drug Discov.* 8 (1) (2013) 49–63.
- [19] B. Caliskan, S. Luderer, Y. Ozkan, O. Werz, E. Banoglu, Pyrazol-3-propanoic acid derivatives as novel inhibitors of leukotriene biosynthesis in human neutrophils, *Eur. J. Med. Chem.* 46 (10) (2011) 5021–5033.
- [20] S. Levent, J. Gerstmeier, A. Olgac, F. Nikels, U. Garscha, A. Carotti, A. Macchiarulo, O. Werz, E. Banoglu, B. Caliskan, Synthesis and biological evaluation of C(5)-substituted derivatives of leukotriene biosynthesis inhibitor BRP-7, *Eur. J. Med. Chem.* 122 (2016) 510–519.
- [21] C. Pergola, J. Gerstmeier, B. Monch, B. Caliskan, S. Luderer, C. Weinigel, D. Barz, J. Maczewsky, S. Pace, A. Rossi, L. Sautebin, E. Banoglu, O. Werz, The novel benzimidazole derivative BRP-7 inhibits leukotriene biosynthesis in vitro and in vivo by targeting 5-lipoxygenase-activating protein (FLAP), *Br. J. Pharmacol.* 171 (12) (2014) 3051–3064.
- [22] S. Shekfeh, B. Caliskan, K. Fischer, T. Yalcin, U. Garscha, O. Werz, E. Banoglu, A Multi-step Virtual Screening Protocol for the Identification of Novel Non-acidic Microsomal Prostaglandin E2 Synthase-1 (mPGES-1) Inhibitors, *ChemMedChem* 14 (2) (2019) 273–281.
- [23] A. Olgac, A. Carotti, C. Kretzer, S. Zergiebel, A. Seeling, U. Garscha, O. Werz, A. Macchiarulo, E. Banoglu, Discovery of novel 5-lipoxygenase-activating protein (FLAP) inhibitors by exploiting a multistep virtual screening protocol, *J. Chem. Inf. Model.* 60 (3) (2020) 1737–1748.
- [24] E. Banoglu, E. Celikoglu, S. Volker, A. Olgac, J. Gerstmeier, U. Garscha, B. Caliskan, U.S. Schubert, A. Carotti, A. Macchiarulo, O. Werz, 4,5-Diarylloxazol-3-carboxylic acids: A new class of leukotriene biosynthesis inhibitors potentially targeting 5-lipoxygenase-activating protein (FLAP), *Eur. J. Med. Chem.* 113 (2016) 1–10.
- [25] U. Garscha, S. Voelker, S. Pace, J. Gerstmeier, B. Emimi, S. Liening, A. Rossi, C. Weinigel, S. Rummmler, U.S. Schubert, G.K. Scriba, E. Celikoglu, B. Caliskan, E. Banoglu, L. Sautebin, O. Werz, BRP-187: A potent inhibitor of leukotriene biosynthesis that acts through impeding the dynamic 5-lipoxygenase/5-lipoxygenase-activating protein (FLAP) complex assembly, *Biochem. Pharmacol.* 119 (2016) 17–26.
- [26] A. Koeberle, U. Siemoneit, U. Buhning, H. Northoff, S. Laufer, W. Albrecht, O. Werz, Licofelone suppresses prostaglandin E2 formation by interference with the inducible microsomal prostaglandin E2 synthase-1, *J. Pharmacol. Exp. Ther.* 326 (3) (2008) 975–982.
- [27] M.G. Chini, R. De Simone, I. Bruno, R. Riccio, F. Dehm, C. Weinigel, D. Barz, O. Werz, G. Bifulco, Design and synthesis of a second series of triazole-based compounds as potent dual mPGES-1 and 5-lipoxygenase inhibitors, *Eur. J. Med. Chem.* 54 (2012) 311–323.
- [28] R. De Simone, M.G. Chini, I. Bruno, R. Riccio, D. Mueller, O. Werz, G. Bifulco, Structure-based discovery of inhibitors of microsomal prostaglandin E2 synthase-1, 5-lipoxygenase and 5-lipoxygenase-activating protein: promising hits for the development of new anti-inflammatory agents, *J. Med. Chem.* 54 (6) (2011) 1565–1575.
- [29] C. Greiner, H. Zettl, A. Koeberle, C. Pergola, H. Northoff, M. Schubert-Zsilavecz, O. Werz, Identification of 2-mercaptohexanoic acids as dual inhibitors of 5-lipoxygenase and microsomal prostaglandin E(2) synthase-1, *Bioorg. Med. Chem.* 19 (11) (2011) 3394–3401.
- [30] M. Hieke, C. Greiner, T.M. Thieme, M. Schubert-Zsilavecz, O. Werz, H. Zettl, A novel class of dual mPGES-1/5-LO inhibitors based on the alpha-naphthyl pirinixic acid scaffold, *Bioorg. Med. Chem. Lett.* 21 (5) (2011) 1329–1333.
- [31] K. Meirer, D. Steinhilber, E. Proschak, Inhibitors of the arachidonic acid cascade: interfering with multiple pathways, *Basic Clin. Pharmacol. Toxicol.* 114 (1) (2014) 83–91.
- [32] O. Radmark, B. Samuelsson, Regulation of the activity of 5-lipoxygenase, a key enzyme in leukotriene biosynthesis, *Biochem. Biophys. Res. Commun.* 396 (1) (2010) 105–110.
- [33] J. Gerstmeier, C. Weinigel, S. Rummmler, O. Radmark, O. Werz, U. Garscha, Time-resolved in situ assembly of the leukotriene-synthetic 5-lipoxygenase/5-lipoxygenase-activating protein complex in blood leukocytes, *FASEB J.* 30 (1) (2016) 276–285.
- [34] O. Werz, 5-lipoxygenase: cellular biology and molecular pharmacology, *Curr. Drug Targets Inflamm. Allergy* 1 (1) (2002) 23–44.
- [35] D. Riendeau, R. Aspiotis, D. Ethier, Y. Gareau, E.L. Grimm, J. Guay, S. Guiral, H. Juteau, J.A. Mancini, N. Methot, J. Rubin, R.W. Friesen, Inhibitors of the inducible microsomal prostaglandin E2 synthase (mPGES-1) derived from MK-886, *Bioorg. Med. Chem. Lett.* 15 (14) (2005) 3352–3355.
- [36] K.M. Partridge, S. Antony, S.N. Bhattachar, S. Chandrasekhar, M.J. Fisher, A. Fretland, K. Gooding, A. Harvey, N.E. Hughes, S.L. Kuklish, J.G. Luz, P. R. Manninen, J.E. McGee, D.R. Mudra, A. Navarro, B.H. Norman, S.J. Quimby, M. A. Schiffler, A.V. Sloan, A.M. Warshawsky, J.M. Weller, J.S. York, X.P. Yu, Discovery and characterization of [(cyclopentyl)ethyl]benzoic acid inhibitors of microsomal prostaglandin E synthase-1, *Bioorg. Med. Chem. Lett.* 27 (6) (2017) 1478–1483.
- [37] N.C. Gilbert, W.E. Boeglin, A.R. Brash, M.E. Newcomer, The Structure of Human 5-Lipoxygenase, 217(2011) (2011).
- [38] A.D. Ferguson, B.M. McKeever, S. Xu, D. Wisniewski, D.K. Miller, T.-T. Yamin, R. H. Spencer, L. Chu, F. Ujjainwalla, B.R. Cunningham, J.F. Evans, J.W. Becker, Crystal structure of inhibitor-bound human 5-lipoxygenase-activating protein 317 (2007) 510–512.
- [39] S. Salentin, S. Schreiber, V.J. Haupt, M.F. Adasme, M. Schroeder, PLIP: fully automated protein-ligand interaction profiler, *Nucleic Acids Res.* 43 (W1) (2015) W443–W447.
- [40] The PyMOL Molecular Graphics System, Schrödinger, LLC.
- [41] M.A. Lomize, A.L. Lomize, I.D. Pogozheva, H.I. Mosberg, OPM: orientations of proteins in membranes database, *Bioinformatics* 22 (5) (2006) 623–625.
- [42] M. Boccellino, M. Donniacuo, F. Bruno, B. Rinaldi, L. Quagliuolo, M. Ambrusi, S. Pace, M. De Rosa, A. Olgac, E. Banoglu, N. Alessio, A. Massa, H. Kahn, O. Werz, A. Fiorentino, R. Filosa, Protective effect of piceatannol and bioactive stilbene derivatives against hypoxia-induced toxicity in H9c2 cardiomyocytes and structural elucidation as 5-LOX inhibitors, *Eur. J. Med. Chem.* 180 (2019) 637–647.
- [43] F. Bruno, S. Errico, S. Pace, M.B. Nawrozkij, A.S. Mkrtychyan, F. Guida, R. Maisto, A. Olgac, M. D'Amico, S. Maione, M. De Rosa, E. Banoglu, O. Werz, A. Fiorentino, R. Filosa, Structural insight into the optimization of ethyl 5-hydroxybenzo[g]indol-3-carboxylates and their bioisosteric analogues as 5-LO/m-PGES-1 dual inhibitors able to suppress inflammation, *Eur. J. Med. Chem.* 155 (2018) 946–960.
- [44] Z.T. Gur, B. Caliskan, U. Garscha, A. Olgac, U.S. Schubert, J. Gerstmeier, O. Werz, E. Banoglu, Identification of multi-target inhibitors of leukotriene and prostaglandin E2 biosynthesis by structural tuning of the FLAP inhibitor BRP-7, *Eur. J. Med. Chem.* 150 (2018) 876–899.
- [45] C.A. Winter, E.A. Risley, G.W. Nuss, Carrageenin-induced edema in hind paw of the rat as an assay for antiinflammatory drugs, *Proc. Soc. Exp. Biol. Med.* 111 (1962) 544–547.
- [46] Schrödinger Release 2017-1: Maestro, Schrödinger, LLC, New York, NY, 2017.
- [47] Schrödinger Release 2017-1: Schrödinger Suite 2017-1 Protein Preparation Wizard; Epik, Schrödinger, LLC, New York, NY, 2017; Impact, Schrödinger, LLC, New York, NY, 2017; Prime, Schrödinger, LLC, New York, NY, 2017.
- [48] Schrödinger Release 2017-1: LigPrep, Schrödinger, LLC, New York, NY, 2017.
- [49] Schrödinger Release 2017-1: Glide, Schrödinger, LLC, New York, NY, 2017.
- [50] R.A. Friesner, J.L. Banks, R.B. Murphy, T.A. Halgren, J.J. Klicic, D.T. Mainz, M.P. Repasky, E.H. Knoll, M. Shelley, J.K. Perry, D.E. Shaw, P. Francis, P.S. Shenkin, Glide: A new approach for rapid, accurate docking and scoring. 1. Method and assessment of docking accuracy, *J. Med. Chem.* 47(7) (2004) 1739–1749.
- [51] T.A. Halgren, R.B. Murphy, R.A. Friesner, H.S. Beard, L.L. Frye, W.T. Pollard, J. L. Banks, Glide: a new approach for rapid, accurate docking and scoring. 2. Enrichment factors in database screening, *J. Med. Chem.* 47 (7) (2004) 1750–1759.
- [52] T.A. Halgren, R.B. Murphy, R.A. Friesner, H.S. Beard, L.L. Frye, W.T. Pollard, J. L. Banks, Glide: A new approach for rapid, accurate docking and scoring. 1. Method and assessment of docking accuracy, *J. Med. Chem.* 47 (7) (2004) 1750–1759.
- [53] <https://github.com/pharmai/plip/blob/v1.4.4/DOCUMENTATION.md> (Accessed on 1 December 2020).
- [54] <https://github.com/pharmai/plip/blob/v1.4.4/plip/modules/config.py> (Accessed on 1 December 2020).
- [55] D.J. Barlow, J.M. Thornton, Ion-pairs in proteins, *J. Mol. Biol.* 168 (4) (1983) 867–885.
- [56] G.B. McGaughey, M. Gagne, A.K. Rappe, pi-Stacking interactions. Alive and well in proteins, *J. Biol. Chem.* 273 (25) (1998) 15458–15463.
- [57] Schrödinger Release 2017-1: Desmond Molecular Dynamics System, New York, NY, 2017. Maestro-Desmond Interoperability Tools, Schrödinger, New York, NY, 2017.
- [58] C.H. Huang, J.R. Lapidus, I.W. Levin, Phase-transition behavior of saturated, symmetric chain phospholipid bilayer dispersions determined by Raman spectroscopy: correlation between spectral and thermodynamic parameters, *J. Am. Chem. Soc.* 104 (22) (1982) 5926–5930.
- [59] W. Humphrey, A. Dalke, K. Schulten, VMD: visual molecular dynamics, *J. Mol. Graph* 14(1) (1996) 33–8, 27–8.
- [60] M.J. Abraham, T. Murtola, R. Schulz, S. Pall, J.C. Smith, B. Hess, E. Lindahl, GROMACS: High performance molecular simulations through multi-level parallelism from laptops to supercomputers, *SoftwareX* 1–2 (2015) 19–25.